Plasma Sci. Technol. **25** (2023) 055502 (15pp) https://doi.org/10.1088/2058-6272/acab42

The influence of pore characteristics on rock fragmentation mechanism by high-voltage electric pulse

Weiji LIU (刘伟吉)[1,2,*], **Youjian ZHANG** (张有建)[1], **Xiaohua ZHU** (祝效华)[1,2] **and Yunxu LUO** (罗云旭)[1]

[1] School of Mechatronic Engineering, Southwest Petroleum University, Chengdu 610500, People's Republic of China
[2] Geothermal Energy Research Center, Southwest Petroleum University, Chengdu 610500, People's Republic of China

E-mail: lwj2017_swpu@163.com

Received 31 October 2022, revised 17 November 2022
Accepted for publication 13 December 2022
Published 21 February 2023

Abstract

High-voltage electric pulse (HVEP) is an innovative low-energy and high-efficiency technique. However, the underlying physics of the electrical breakdown within the rock, and the coupling mechanism between the various physical fields involved in HVEP still need to be further understood. In this study, we establish a 2D numerical model of multi-physical field coupling of the electrical breakdown of porous rock with randomly distributed pores to investigate the effect of pore characteristics (porosity, pore media composition) on the partial electrical breakdown of rock (i.e. the generation of a plasma channel inside the rock). Our findings indicate that the generation of a plasma channel is directionally selective and extends in the direction of a weak electrical breakdown intensity. As the porosity of the rock increases, so does the intensity of the electric field in the 'electrical damage' region—the greater the porosity, the greater the effectiveness of rock-breaking. As the fraction of pore fluid (S_{water}/S_{air}) gradually declines, the generation time of the plasma channel decreases, and the efficacy of rock-breaking by HVEP increases. In addition, in this study, we conducted an indoor experiment utilizing an electric pulse drill to break down the rock in order to recreate the growth mode of the plasma channel in the rock. Moreover, the experimental results are consistent with the simulation results. In addition, the development of this type of partial electrical breakdown is confirmed to be related to electrode polarity and pore characteristics via the experiment of the symmetrical needle-needle electrode arrangement, which further demonstrates the mechanism of partial electrical breakdown. This research is significant for comprehending the process of electric impulse rock-breaking and gives theoretical guidance and technological support for advancing electric impulse drilling technology.

Keywords: high-voltage electric pulse, pore characteristics, electrical breakdown, porous rock, plasma channel, electrical breakdown test

(Some figures may appear in colour only in the online journal)

1. Introduction

The efficiency of drilling and rock-breaking determines the economics of project operation from deep geo-energy resources (e.g. geothermal, oil and gas) because drilling expenses account for the bulk of total project expenditures [1, 2]. In addition, the expense of drilling operations increases exponentially as the drilling depth increases [3–5]. High-voltage electric pulse (HVEP) drilling technology stands out due to its advantages, which include high rock-breaking

* Author to whom any correspondence should be addressed.

efficiency, good wellbore quality, green environmental protection, directional rock-breaking and easy control of the rock-breaking process, as well as the fact that its drilling cost is not limited by drilling depth. It is considered to be a new green rock-breaking technology with enormous growth potential [6–9]. At present, HVEP drilling technology is a new rock-breaking technique that is almost ready for industrialization [10–12], and its viability has been proved by researchers from numerous nations [13, 14]. However, the complex characteristics of rock strata encountered in the process of electric pulse rock-breaking, particularly the influence of rock pore characteristics on the mechanism of electric pulse rock-breaking, are insufficiently understood. The mechanism of rock-breaking by coupling multiple physical fields involved is difficult to describe precisely, which limits the industrial application of HVEP technology to some degree.

HVEP drilling technology can be divided into two categories based on its rock-breaking mechanism: hydraulic electric rock-breaking and electric pulse rock-breaking [15–19]. Hydroelectric rock-breaking occurs when the rise time of the pulse voltage is long or the insulating quality of the liquid insulating medium is weak. Since the electrode immersed in the liquid media does not directly make contact with the rock surface, its discharge channel will be produced directly in the liquid medium. The shock-wave stress produced when the liquid medium is electrically broken will break the rock [20–23]. In comparison, electric pulse rock-breaking generally penetrates the rock when its voltage rise time delay is shorter than 500 ns, and the electrode is in direct contact with the rock. At this point, the rock's breaking strength is less than that of the liquid medium. The rock is preferentially broken down by electricity, generating a plasma channel within its interior. Due to the shock-wave force generated when the plasma channel sprouts, the rock fractures [24–27].

Rock is a complex porous medium in which pores belong to the mechanical fracture of the rock. These pores are the outcome of the strain caused by stress concentration on faults, heterogeneity, and physical discontinuities [28, 29], which can exist in various sizes, from large plates to microscopic particles. Porosity, which refers to the ratio of pore space to total volume, is one of the fundamental physical properties of rocks [30, 31]. The existence of pores in the rock modifies the rock's electric field during HVEP drilling, and the electric field strength is greatest at the intersection of pores and rock matrix. Consequently, the electric vein breaks the rock preferentially along the border of the pores [32, 33]. In the phenomenon known as 'partial discharge breakdown', an electrical breakdown occurs in a single rock pore, resulting in considerable pore pressure and rock fracture [34, 35]. In recent decades, several scholars have explored how the existence of natural or unnatural pores or cracks in rock impacts the partial electrical breakdown of the rock during the electric pulse rock-breaking approach [36, 37]. Granite and concrete that have been treated with bubbles cannot be broken down, whereas granite and concrete that have not been treated can be broken down. Experiments demonstrate that when a porous rock is subjected to a high-voltage electric field, the pore cavity will rupture, and the current will transfer and conduct to the gas cavity, resulting in the development of multiple amounts of plasma heat and high-pressure pulse waves. The pulse pressure will cause the formation of cracks and rock fragmentation. The rock's porosity significantly affects the intensity of the breakdown field. The breakdown field intensity reduces as the porosity increases [38–45]. In addition, it contains a variety of fluid media, because the pore space within the rock is enclosed. Under the same pulse voltage, a dry granite sample will be broken down by electricity more easily than a water-saturated granite sample. Furthermore, the dry rock sample will have a more obvious broken effect [46].

To investigate the effect of pore characteristics on the electric pulse rock-breaking process, this paper focuses on the distribution of numerous pores in the rock, the change in porosity and the effect of fluid medium distribution ratio in the pores. First, we briefly introduce the process of electric pulse drilling and the principle of electrical breakdown. Next, we construct a rock model with a random distribution of numerous pores and a 2D numerical model of multi-physical field coupling electrical breakdown of porous rocks. We mainly study the effect of pore characteristics (porosity, pore fluid and proportion of pore-fluid distribution) on the partial electrical breakdown of rocks (plasma formation in rocks). Finally, is this study, we also conducted an indoor experiment of electric pulse drilling to break through rock, reproduced the growth mode of the plasma channel within the rock, and then conducted the needle-needle electrode electrical breakdown experiment to investigate the distinction between the high-voltage electrode and the low-voltage electrode in the process of electric pulse drilling through rock. Consistent with the conclusions of the simulation tests, the results of the two electrical breakdown investigations verify the process by which an electric pulse shatters rock.

2. HVEP drilling technology

HVEP drilling is a non-contact drilling technology that utilizes high-voltage electric pulses to fracture rock without causing mechanical wear. Electrical breakdown of rock is a complicated process, and rock-breaking by electric pulses can be divided into two modes: electric pulse rock-breaking and hydroelectric rock-breaking. Electrical breakdown in rock occurs when the rise time of the electric pulse is less than 500 ns, and the breakdown field strength decreases from water to rock to air [12].

Currently, the plasma channel is generated inside the rock, and the resultant stress wave immediately acts on the surrounding rock, resulting in a rapid rate of rock-breaking. While this demonstrates that the HEVP drilling method is highly effective, its practical application is hindered by standard drilling settings. Particularly difficult is the fact that the electrodes that give the HVEP must be in direct contact with the rock surface, as depicted in figure 1. The HEVP rock-breaking process consists primarily of three stages: stage I is plasma generation, stage II is initial plasma channel construction and stage III is rock-breaking. Initially, electric pulses inject electrical energy into rock. In stage I, the electric

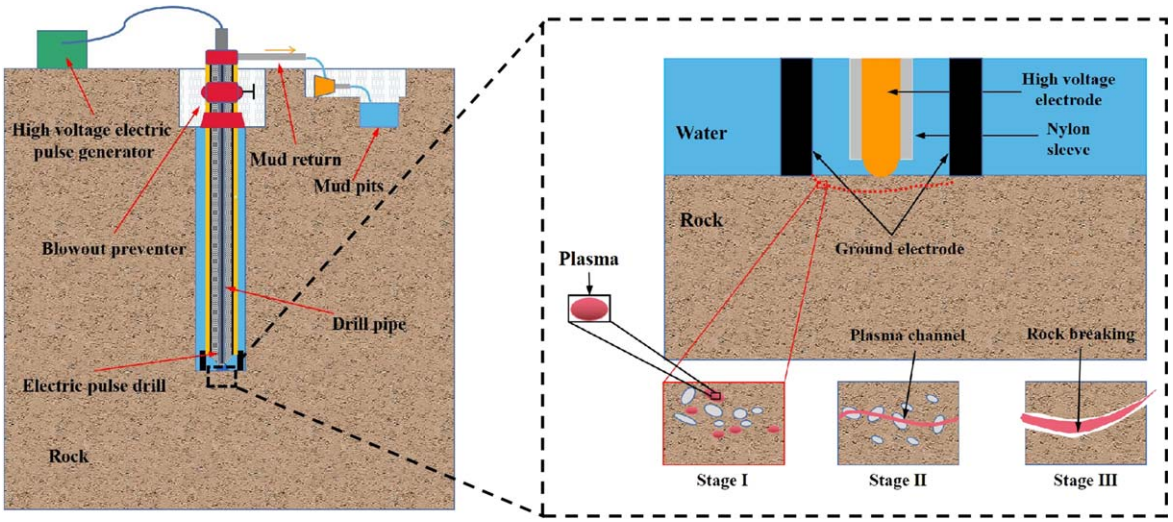

Figure 1. Schematic diagram of the rock-breaking stage of the HVEP drilling process.

field intensity of the HVEP-affected area will induce a distortion effect, and a small amount of plasma will be produced. In stage II, the pores in the rock will undergo electrical breakdown due to the continuous action of the HVEP, the plasma channel will generate progressively through the pores alongside the production of cracks in the rock, and a plasma channel will eventually be generated. In stage III, the HVEP-generated current will continue to inject into the plasma channel. Meanwhile, it will generate tremendous heat and a high-intensity force in the vicinity of the channel. Eventually, penetrating pores will form, causing the rock to be fractured from the inside, and the insulating drilling fluid will remove the shattered rock to prevent repeated breakage, thereby achieving HVEP rock-breaking. In HVEP drilling, there is an exponential power relationship between breakdown voltage and electrode spacing, and the system's energy efficiency is proportional to the electrode spacing. The porosity of the rock has a significant impact on the intensity of the electrical breakdown field.

3. 2D electrical breakdown model of porous rock

3.1. Establishment of porous rock model

The HVEP drilling process encounters a formation that contains a range of spatial pores. These microscopic pores serve as reservoir space and seepage channels in reservoir rocks. Furthermore, the presence of a significant number of pores influences the macroscopic mechanical state of rock and plays a crucial role in influencing rock failure. The pores may hold a range of substances, including air, natural gas and water. Therefore, this paper proposes a 2D electrical breakdown model of porous rock, coupling the electric field, temperature field, flow field and stress field, to examine the effect of the porosity and the medium composition in pores on the rock fragmentation behavior induced by HVEP. In the rock model, various pores are randomly distributed and are filled with media (air, natural gas and water). The peculiarity of the

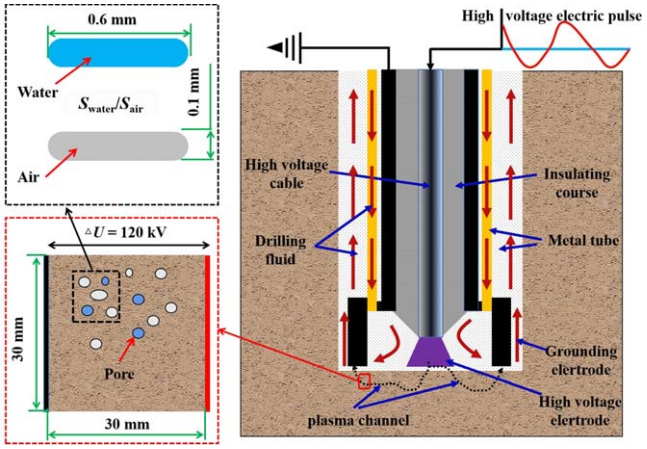

Figure 2. Schematic diagram of numerical the simulation model for partial breakdown of multi-pore rock current field.

electrical breakdown model provided in this research is that it considers the random distribution of pores in the rock, the geometry of pores, the porosity value and the distribution ratio of pore fluids when analyzing the electrical breakdown phenomenon of rock.

As indicated in figure 2, a numerical simulation model of the partial breakdown of the current rock field in porous, and thus non-conductive material presents. During the partial electrical breakdown induced by the plasma channel, we select a tiny square with an area of 30 mm × 30 mm in the lower left section of figure 2. Multiple pores with randomly generated shapes, sizes and positions are positioned in the micro-element body's center; the pores are elliptical. The random distribution of pores in the micro-body corresponds more accurately to the complex distribution of pores in the rock. In addition, the shortest semi-axis of the smallest pore measures 0.1 mm, while the shortest semi-axis of the largest pore measures 0.3 mm; the smallest long semi-axis of the pore measures 0.3 mm, while the longest semi-axis of the most extensive pore measures 0.6 mm.

Table 1. Four different porosities of rock.

Scheme code	Porosity of rock
A	2%
B	3%
C	4%
D	5%

As shown in table 1, rock models with porosities of 2%, 3%, 4% and 5% were constructed to investigate the impact of porosity on partial electrical breakdown.

These randomly generated pores contain either air or water. To characterize the volume fraction of the particular fluid i in porous rocks, the notion of saturation S_i, which is defined as follows, must be applied:

$$S_i = \frac{V_i}{V_\mathrm{p}}, \tag{1}$$

where V_i is the total volume of a certain fluid i, in mm^3, and V_p represents the total volume of pores in porous rocks, in mm^3.

The definition of saturation is fluid volume divided by pore volume, with fraction or percentage as its unit. In this study, a 2D electrical breakdown model of porous rock is developed to represent the fluid volume i by its area A_i and the pore volume A_p. In the 2D electrical breakdown model, the formula for pore-fluid saturation S_i' is given as,

$$S_i' = \frac{A_i}{A_\mathrm{p}}. \tag{2}$$

Two saturation concepts characterize porous rock models containing water and air/natural gas, with the sum of the two types of pore-fluid saturation equation (1),

$$S_\mathrm{water} + S_\mathrm{air} = 1. \tag{3}$$

Table 2 presents seven distinct schemes of fluid proportion in pores to investigate the influence of medium types in pores on the electrical breakdown of rock.

Table 2. Composition scheme of medium in pores.

Scheme code	Types of media	$S_\mathrm{water}/S_\mathrm{air}$
1	One medium	∞
2		0
3	Two media	4:1
4	Two media	3:2
5	Two media	1:1
6	Two media	2:3
7	Two media	1:4

3.2. Establishment of electrical breakdown model

3.2.1. Governing equations of current field. The process of electrical breakdown can be considered quasi-static, and the electric field iterations in the rock domain and the liquid media domain are governed by Maxwell's equation:

$$\mathbf{J} = \sigma\mathbf{E} + \frac{\partial \mathbf{D}}{\partial t}, \tag{4}$$

$$\mathbf{D} = \varepsilon_0\varepsilon_\mathrm{r}\mathbf{E}, \tag{5}$$

$$\frac{\partial \rho_\mathrm{q}}{\partial t} = \nabla \cdot \mathbf{J}, \tag{6}$$

$$\mathbf{E} = -\nabla\varphi, \tag{7}$$

where $\mathbf{D}$ is the electric displacement vector; $\mathbf{J}$ is the current density vector; $\mathbf{E}$ is the electric field strength vector; σ is the electrical conductivity, S m^{-1}; t is the time, s; ε_0 is the vacuum permittivity, its value is 8.854×10^{-12} F m^{-1}; ε_r is the relative permittivity of the medium (rock, electrode and insulating liquid); φ is the electric potential, V; ρ_q is the space charge density, C m^{-3}.

3.2.2. Governing equations of electrical breakdown field. In the process of electrical breakdown, the electrical property of rock lies between resistance and ideal conductor. When the electric field strength within the rock is less than its internal breakdown intensity, it is characterized as resistance in this paper; when a plasma channel is formed in the rock, it is a conductor. In this instance, the rock state transition is represented by the state quantity D_r, between 0 and 1. When $D_\mathrm{r} = 0$, the rock is regular rock (electrical resistance). When $D_\mathrm{r} = 1$, the rock has completed its metamorphosis into a plasma state. In addition, the state variable D_p of the porous medium is introduced, which affects the electrical breakdown field in a similar way to the rock domain state variable D_r. There is a threshold field intensity E_c throughout the electrical breakdown process. Only when the electric field strength within the rock exceeds this threshold can the rock be split apart. Due to the duration of the breakdown process, a hysteresis effect can be observed on the time scale of the breakdown process.

This study concludes that a particular electrical breakdown process must satisfy the following conditions: (1) the partial electric field in the rock exceeds its partial electric field intensity $|E_\mathrm{c}|$; (2) the time of the electric field intensity vector exceeding its local electric field intensity $|E_\mathrm{c}|$ reaches a specific limit 0, in which the boundary time indicates that the energy accumulation in the rock interior during the electrical breakdown process has reached a specific limit (such as phase transition, charge transfer and accumulation). Consequently, in conjunction with the proposed state variable D_r, the control equation (8) for the electrical breakdown field in this study is,

$$\frac{\mathrm{d}D_\mathrm{e}}{\mathrm{d}t} = \frac{1}{\tau_0}\,\mathrm{sgn}[F(|E| - |E_\mathrm{c}|)] \quad (D_\mathrm{e} < 1), \tag{8}$$

where $|E|$ is the electric field strength, V m^{-1}; $|E_\mathrm{c}|$ is the partial electric field intensity, V m^{-1}, which is the quantity related to the rock properties (such as internal pore structure, mineral types, components, etc) and it is a function related to the spatial distribution of the rock and is the permeability of the rock. τ_0 is the hysteresis time in seconds; the initial value of D_r, which represents the state change of rock after electrical breakdown, is 0; F and sgn are, respectively, logical and

symbolic functions,

$$F(a) = \begin{cases} 1, & a \geqslant 0 \\ 0, & a < 0 \end{cases}, \tag{9}$$

$$\mathrm{sgn}(b) = \begin{cases} 1, & b > 0 \\ 0, & b = 0 \\ -1, & b < 0 \end{cases}, \tag{10}$$

where a and b are the respective independent variables (input parameters) of the logical function F and the symbolic function sgn.

Various mineral components should have different values for the threshold breakdown field intensity E_c. When a plasma channel is generated in an electrostatic field, the electric field energy comprises two forms of energy: electrostatic energy and electric-mechanical energy [47]. We can express electrostatic energy density w_e as,

$$w_e = \frac{1}{2}\mathbf{D} \cdot \mathbf{E}, \tag{11}$$

where w_e is the electrostatic energy density, J m^{-3}; $|\mathbf{E}|$ is the electric field strength vector, V m^{-1}; $|\mathbf{D}|$ is the electric displacement vector, C m^{-2}.

The electric-mechanical energy density w_m in the plasma channel can be expressed as,

$$w_m = \frac{1}{2}\sigma_m \gamma, \tag{12}$$

where w_m is the electric-mechanical energy density, J m^{-3}; σ_m is the Maxwell stress, which can be expressed as $\sigma_m = \varepsilon_0\varepsilon_r|\mathbf{E}|^2/2$; γ is the strain, the relationship between it and the stress is $\gamma = \sigma_m/E_t$, and E_t is the elastic modulus.

Then, the total energy density w_{em} of the electric field is,

$$w_{em} = \frac{{\varepsilon_0}^2{\varepsilon_r}^2\,|\mathbf{E}|^4}{8E_t} + \frac{\varepsilon_0\varepsilon_r\,|\mathbf{E}|^2}{2}. \tag{13}$$

The start of the plasma channel requires an applied electric field to overcome the volume energy w_f equivalent to the rock's surface energy. Therefore, when w_{em} is exactly equal to w_f, the electric field strength is equal to the threshold breakdown field strength E_c at which a partial electrical breakdown can occur:

$$\frac{{\varepsilon_0}^2{\varepsilon_r}^2{E_c}^4}{8E_t} + \frac{\varepsilon_0\varepsilon_r{E_c}^2}{2} = w_f, \tag{14}$$

where w_f is the volume energy density threshold, J m^{-3}.

The formula for calculating the threshold breakdown field strength E_c is as follows:

$$E_c = \left[\frac{2}{\varepsilon_0\varepsilon_r}\left(\sqrt{{E_t}^2 + 2E_t{w_f}^2} - E_t\right)\right]^{\frac{1}{2}}. \tag{15}$$

According to the electrical breakdown experiments of Boev *et al* [38, 39] and Andres [20, 21], the relationship between the breakdown time delay τ_0 and (nominal) electrical breakdown strength is approximately exponential. In this paper, with the help of their experimental results, the relationship between the breakdown time delay and (nominal) electrical breakdown strength is characterized by the exponential linear combination, namely,

$$\tau_0 = A + B_1 e^{-E_m/C_1} + B_2 e^{-E_m/C_2}, \tag{16}$$

where E_m is the nominal intensity, V m^{-1}; A, B_1, B_2, C_1 and C_2 are constants fitted from experimental data. The nominal breakdown intensity E_m is a nominal and measurable macroscopic quantity, which is roughly the potential difference $\Delta\varphi$ between the high-voltage electrode and the grounding electrode and electrode spacing L_s, i.e.,

$$E_m = \frac{\Delta\varphi}{L_s} = \frac{\varphi_d}{L_s}, \tag{17}$$

where $\Delta\varphi$ is the potential difference between the high-voltage electrode and the grounding electrode, V; φ_d is the potential of the high-voltage electrode, V; L_s is the electrode spacing, m.

The values of other parameters in the electrical breakdown model are $\sigma_{max} = 4 \times 10^7$ S m^{-1}, $\varepsilon_{max} = 206$, in formula (16). The parameter values of rock and water area are shown in table 3.

Table 3. Values of parameters of rock and water in formula (16).

Parameter	Rock field	Water field
A	6.674×10^{-8}	7.84861×10^{-8}
B_1	6.60795×10^{-5}	2.13147×10^{-6}
B_2	0.72623	1.40643×10^{-6}
C_1 (V m^{-1})	1.6598×10^6	1.35996×10^6
C_2 (V m^{-1})	325167.72199	7.56997×10^6

3.2.3. Electrical breakdown strength of pore fluids. When the HVEP rock-breaking feature is enabled, the rock will undergo partial electrical breakdown, and the pores within the rock will also undergo electrical breakdown. The partial electric field strength operating on the pores is greater than the electric field intensity of the internal medium, which is the basis for the electrical breakdown of the pores. It is essential to first determine the degree of electrical breakdown in the pores of the medium, when developing the 2D model of electrical breakdown.

3.2.3.1. Electrical breakdown strength of air. The electrical breakdown strength of air can be obtained by Paschen's law [48]:

$$V_a(P_p, d_p) = \frac{BP_pd_p}{\ln(AP_pd_p) - \ln\left[\ln\left(1 + \frac{1}{\gamma_{sec}}\right)\right]}, \quad (d_p > 10\ \mu\mathrm{m},\ P_p < 2.5\ \mathrm{MPa}). \tag{18}$$

We can calculate the breakdown voltage V_a of any gas (e.g. air), given the pore pressure P_p and micro-pore size d_p. $A = 9$ Pa m^{-1} and $B = 256.5$ Pa m^{-1} are the first and second constants of the Paschen curve, respectively, in equation (18).

Table 4. Electrode, water and insulating sleeve material properties.

Material	Relative permittivity	Electrical conductivity (S m^{-1})	Specific heat capacity (J kg^{-1} K^{-1})	Density (kg m^{-3})	Thermal conductivity (W m^{-1} K^{-1})
Water	80	0.00125	4180	1000	0.59
Electrode	1	5.7×10^7	385	8960	400
Insulating sleeve	4	0	1700	1150	0.26

These constants are specific to air and have been determined through pertinent experiments [49]. At the same time, the secondary ionization coefficient γ_{sec} has been experimentally found and ranges from 0.01–0.05 for the dielectric boundary (e.g. rock grains) and electrical conductor boundaries, respectively [49]. However, Paschen's law is a semi-empirical formulation, and for pores smaller than 10 μm, the electrical breakdown criteria deviate from Paschen's law, limiting our model to micro-pore sizes more than 10 μm (i.e. $d_p > 10\ \mu$m) [50, 51].

In this paper, we use the dielectric strength E_a of air instead of the breakdown voltage. Incorporating the applied voltage and the gap distance (pore size) into a single parameter simplifies the problem analysis. Therefore, to calculate the electrical breakdown strength of air, we divide both sides of the classic Paschen's law by the pore size d_p to obtain,

$$E_a(P_p, d_p) = \frac{BP_p}{\ln(AP_p d_p) - \ln\left[\ln\left(1 + \frac{1}{\gamma_{sec}}\right)\right]}, \quad (d_p > 10\ \mu\text{m},\ P_p < 2.5\ \text{MPa}). \tag{19}$$

3.2.3.2. Electrical breakdown strength of water. The electrical breakdown strength of water can be obtained by Martin's empirical formula [43]:

$$\begin{cases} E_w + = \dfrac{K}{t_b{}^{1/3} \times S^{1/10}} \\ E_w - = \dfrac{K}{t_b{}^{1/3} \times S^{1/10}} \end{cases} \quad \begin{pmatrix} t_b \geqslant 50\ \text{ns}; \\ \text{Positive voltage } K = 0.3, \\ \text{Negative voltage } K = 0.6 \end{pmatrix}, \tag{20}$$

where E_w+ and E_w- are the breakdown field strengths of water (MV cm^{-1}) and related to the electrode polarity; S refers to the area of the pore when the medium in the pore is water (cm^2); t_b is defined as the time when the voltage is more than 63% of the maximum voltage. Therefore, the electrical breakdown strength of water may be calculated by equation (20).

3.2.4. 2D electrical breakdown model of porous rock. In HVEP rock-breaking drilling, the electrode bit structure significantly affects the rock-breaking efficiency and energy conversion efficiency. Typically, the electrode arrangement of a drilling bit is coaxial or at an angle to the axis. Regardless of how the electrodes are organized, the rock-breaking unit consists of a 'high-voltage electrode—rock domain—ground electrode' in a 'needle-needle' side-by-side configuration. The two electrodes are positioned symmetrically and surrounded by two insulating sleeves in direct contact with the rock surface. When the discharge voltage reaches 120 kV, this apparatus is part of the electric pulse rock-breaking mechanism mentioned previously.

The distribution of shape, size and placement of the pores within the rock's interior is arbitrary. In addition, both electrodes are situated on the same side of the rock. The length of the electrode and the distances between the two electrodes are 10 and 20 mm, whereas the width and depth of the rock are 30 and 30 mm, respectively. In addition, an insulating material is wrapped around the electrode to prevent electrical leakage from the electrode's non-end. The material characteristics of the electrode, water and insulating sleeve are detailed in table 4.

4. Numerical investigations and analysis of HVEP drilling technology

4.1. Plasma channel generation process and channel conductivity distribution

Figure 3 displays the formation process of the plasma channel when the pore medium of model A is entirely air. D_r and D_p represent the rock state variable and the pore state variable, respectively. The plasma channel in the rock does not generate directly from the end of the electrode but instead begins to sprout near the end of the electrode. During a period of 0–700 ns, the electric field intensity will be altered where there are pores, initiating 'electrical damage' within the rock and generating plasma channels. The generation of plasma channels has directional features; hence, 'electrical damage' is more likely to appear in the direction of the pores within the rock. Subsequently, between 900–1500 ns, the electric field intensity is relatively weak at many pores, where 'electrical damage' expands and penetrates to generate the initial plasma channel architecture. Ultimately, the energy in the circuit is injected into the rock through the plasma channel, which exacerbates the damage to the rock and ultimately generates the electrical breakdown channel.

Figure 4 portrays the rock's electrical conductivity distribution under conditions of 2%, 3%, 4% and 5% porosities, respectively. When the pore media is air, the plasma channel shape can be observed via the electrical conductivity distribution diagram in figure 4. Typically, plasma channels form in the direction of pores and sprout towards the pores in the rock. The formation path of the channels will pass through the pores

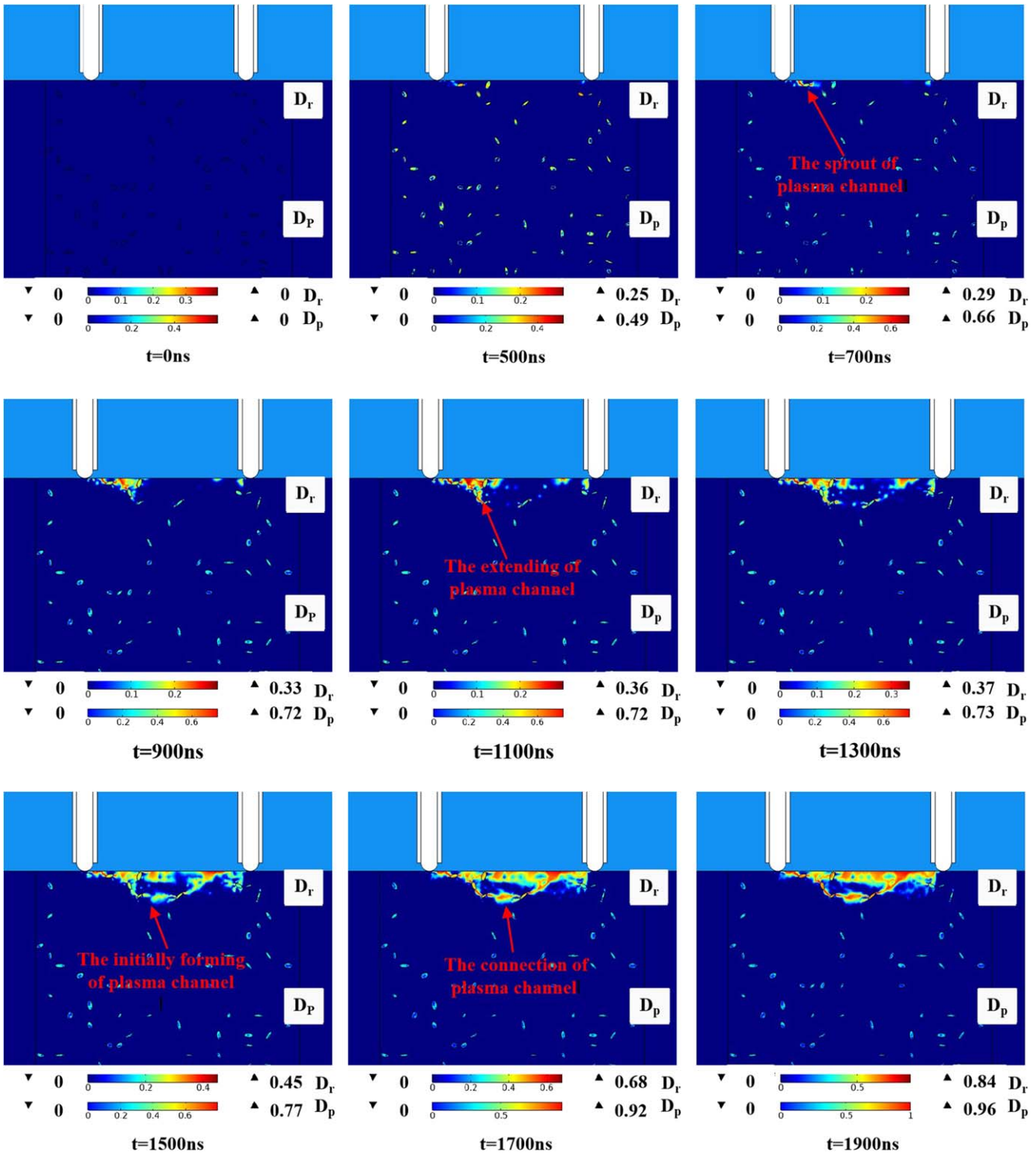

Figure 3. Generation process of plasma channel inside the rock.

because the medium within the pores is air, and the electrical breakdown strength of air is less than that of rock. Therefore, the channels will preferentially extend towards the pores.

4.2. The influence of porosity on partial electrical breakdown

Figure 5 plots the breakdown time and partial electric field strength as a function of porosities. In the simulation, four rock models with varying porosities are established: A, B, C and D; the porosities of these four models grow sequentially. To limit the error caused by the random distribution of pores, four rock models with the same porosity were each developed, for a total of sixteen rock models. Then, the electric pulse simulation test was conducted, and the simulation results were averaged to obtain the electric pulse simulation results of rock with varying porosity, as depicted in figure 5,

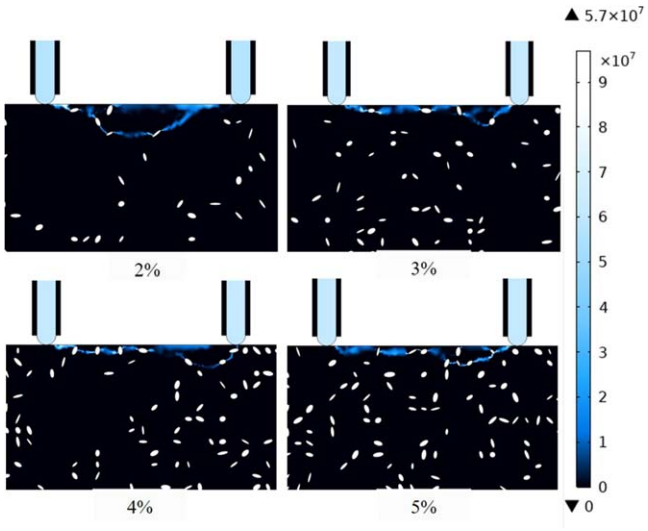

Figure 4. Conductivity distribution in the plasma channel inside rocks with different porosities.

to examine the effect of porosity on partial electrical breakdown within the rock.

Figure 5(a) presents that as the porosity gradually increases, the time of electrical breakdown inside the rock gradually lowers, indicating that the rock is more susceptible to electrical breakdown as the porosity increases. In conjunction with the fact that the plasma channel generation described in section 4.1 has a particular 'direction' and the 'electrical damage' of the rock is also more likely to sprout along the pore direction within the rock, the above analysis indicates that porosity is a significant factor in the HVEP rock-breaking process.

Figure 5(b) demonstrates that while the porosity gradually increases, the partial electric field intensity in the rock model will grow proportionally. Hence, the rock-breaking effect of the HVEP is gradually strengthened, making it relatively simple to perform HVEP rock breakdown. However, as the porosity reaches a specific threshold, the increasing electric field intensity within the rock gradually becomes steady. Consequently, in the actual application of HVEP rock-breaking, the discharge voltage cannot be increased above a specific value, thus conserving energy and achieving maximum efficiency to a certain extent.

4.3. The influence of the proportion of pore fluid on partial electrical breakdown

Figure 6 shows the relationship between the rock's internal state variable (D_r) and different pore-fluid distribution ratios for rock with a 2% porosity. Using the quantified state variable D_r, we can quantitatively assess the rock pores under an electric pulse. Initially, the state variables of the rock are area-integrated, with the computation results treated as the equivalent failure area S_{rock} of the rock domain, i.e. the rock domain's failure zone:

$$S_{rock} = \int D_r \mathrm{d}S, \tag{21}$$

where S_{rock} is the equivalent failure area of the rock domain (m^2); D_r is the state variable of the rock.

According to table 2 in section 3.1, the proportion of fluid in the pores (S_{water}/S_{air}) is split into seven categories. In this section, rock model A is utilized, the elliptical porosity is 2%, and for each pore-fluid ratio, four rocks with the same porosity were formed; a total of 28 rock models were developed. As illustrated in figure 6, the corresponding failure area and breakdown time of the 'electrical damage' area inside the rock were averaged after comparing and analyzing the simulation results of all rock models.

Figure 6 indicates, for a constant porosity, that as the amount of pore fluid decreases, the duration of electrical breakdown within the rock (the time when the plasma channel is completely generated) also decreases accordingly. It reveals that when the medium in the pore contains air, it is easier to have an electrical breakdown, and the more air there is, the easier it is to generate plasma channels. With a change in the amount of fluid in the interior pores of the rock, the comparable failure area of the 'electrical damage' zone will also alter considerably. The rock equivalent failure region is the most miniature, and the electric pulse's rock-breaking effect is weakest when the pore media is saturated with water. As the percentage of pore fluid steadily decreases, the equivalent failure area of the rock increases, demonstrating that when the pore medium includes air, the electric pulse can fracture the rock more efficiently.

Figure 7 reveals the route of the plasma channel formed in the rock at various pore-fluid ratios (S_{water}/S_{air}). After the rock model generates plasma channels under the influence of HVEP, the electrical conductivity within the rock will change dramatically. Hence, the generation path of the plasma channels can be indirectly represented by the electrical conductivity of each point within the rock model.

As shown in figure 7, the generation path of the plasma channel within the rock will change as the percentage of fluid varies. When the fraction of fluid in the pores S_{water}/S_{air} continuously decreases to zero, the conductivity surrounding the channel path and the area of the channel route both increase, indicating an increase in the rock-breaking area and an improvement in the rock-breaking effect. Conversely, when the fluid ratio in the pores S_{water}/S_{air} is infinite, the area of the plasma channel route is the smallest, and there is a minor impact on rock-breaking.

When the only medium in the pores is air, the pores are electrically broken down, and the plasma channel path travels through the pores because the electrical breakdown intensity of air is less than that of rock. However, when the only medium in the pores is water, the pores are not damaged, and the plasma channel path follows the surface of the holes. Therefore, rather than having a fixed generation direction in the 'electrical damage' region of the rock, the development of plasma channels has a 'direction' skewed towards regions where the electrical breakdown strength is weaker in the extension direction.

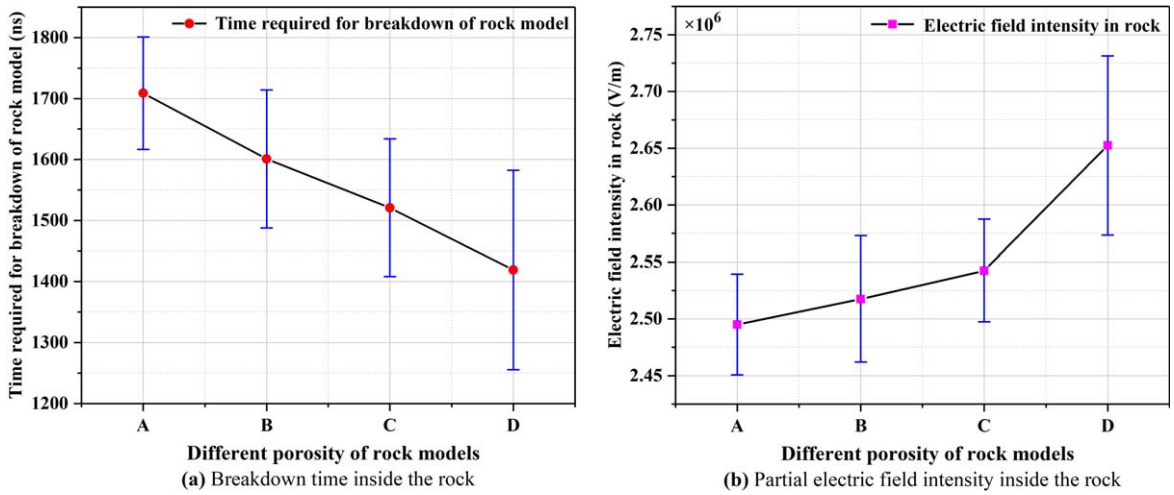

Figure 5. Breakdown time and partial electric field strength of rock with different porosities in the HVEP rock-breaking process.

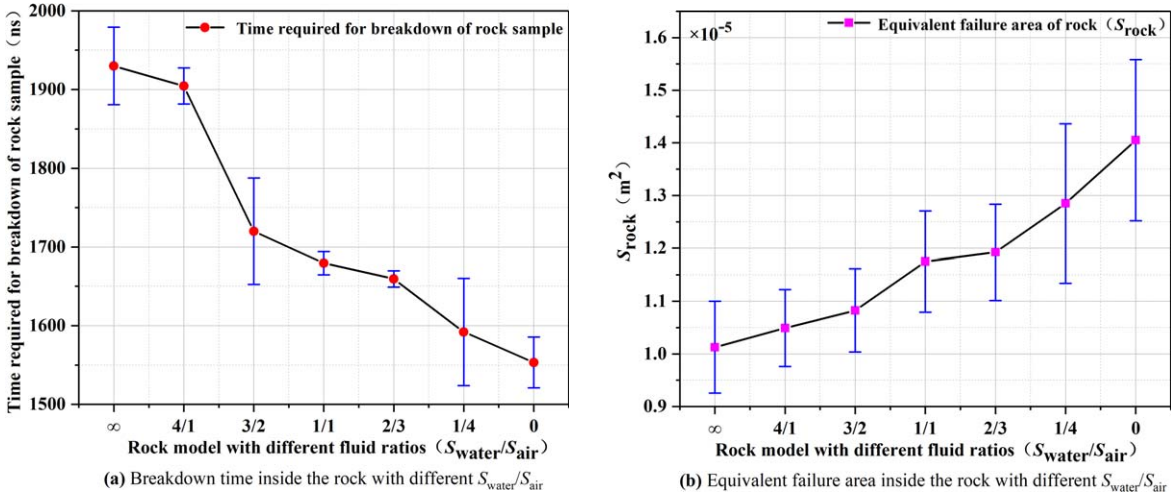

Figure 6. Breakdown time and equivalent failure area inside the rock with different pore-fluid ratios (S_{water}/S_{air}) of rock model samples.

5. HVEP breakdown experiment

Figure 8 displays the experimental setup consisting of an output electrode, four-stage boost device and DC boost power source. Its purpose is to research rock disintegration utilizing HVEP. The DC boost power supply, which also changes commercial frequency AC power supply to DC power supply, performs the initial boost. A four-stage boost structure protects the circuit during the following boost of the circuit and the breakdown of the rock sample. The boost voltage is composed of four capacitors and a number of inductors, and the protection circuit is composed of four air-gap switches and several inductors. Using the output electrode, the instantaneous high-voltage pulse voltage loaded on both ends of the rock sample is discharged. Red and gray sandstones that have been processed into a round cake shape measuring 100 mm in diameter and 10 mm in height are used in the HVEP rock breakdown experiments.

5.1. Evaluation of electrical breakdown test outcomes for an electric pulse drill

The electrode bit used to break the rock sample in experiments can be seen in figure 9. The experiment's fixed output voltage and frequency are 80 kV and 2.5 Hz, respectively. Rock cracking at the HVEP is accompanied by the production of an electric arc and a dull sound. The rock-breaking effect reached the experimental expectation, which is consistent with the outcomes of porous rock's 2D electrical breakdown simulation test. First, the surface of the rock sample develops cracks. Next, under the continuous action of the electric pulse, the HVEP drill bit continues the rock-breaking operation. Finally, the rock sample appears to be completely broken and cracked. Figure 10 clearly shows the HVEP rock-breaking experiment's methodology and outcomes.

Figure 11 exhibits the plasma channel path generated in gray and red sandstone, respectively, due to HVEP rock-breaking. The rock sample has clear break paths, which

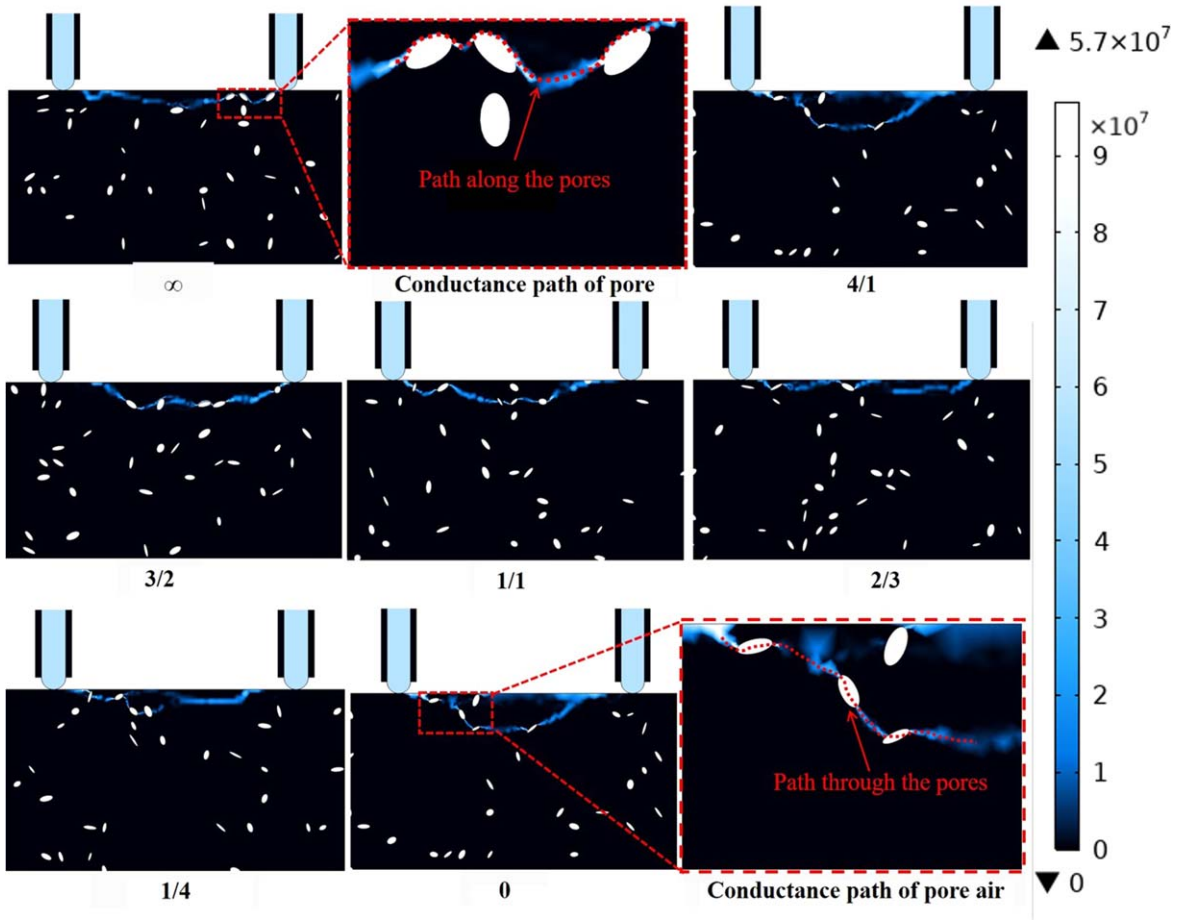

Figure 7. Path diagram of the plasma channel in the rock with different pore-fluid ratios (S_{water}/S_{air}).

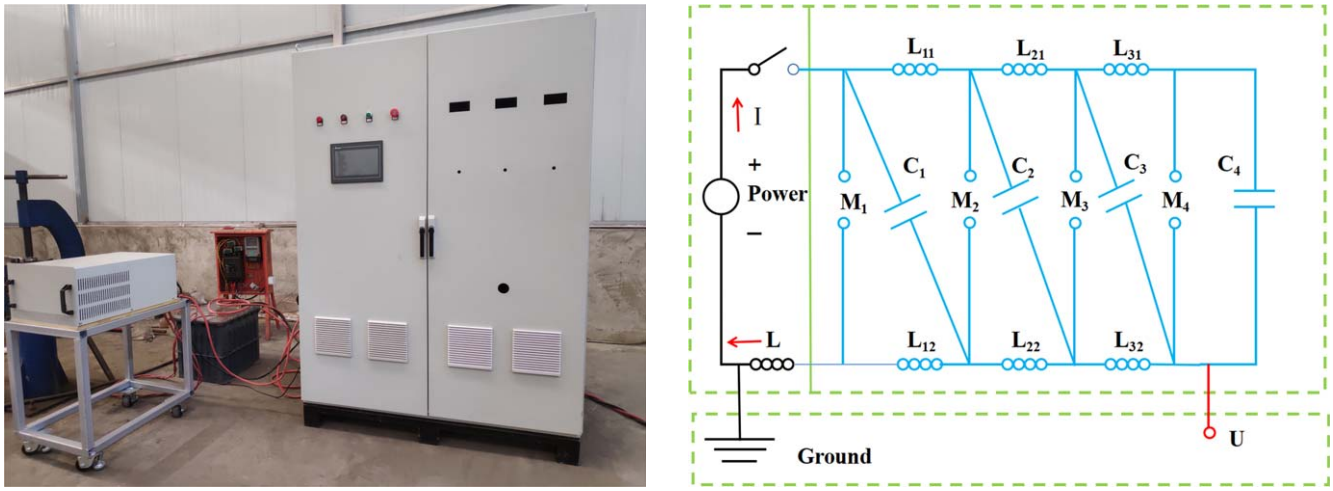

Figure 8. Experimental setup and its simplified circuit structure.

correspond to the plasma channel path. The plasma channel generated in the rock is compatible with the simulation-derived damage path of the rock. Due to the tremendous energy (heat) in the channel, the rock along the course of the plasma channel has a distinct color variation from the surrounding rock. In addition, there are ablative markings surrounding the electrode because, after the construction of the channel, electric energy will continue to be injected to raise the temperature, producing partial thermal damage to the rocks next to the electrode.

5.2. Evaluation of the needle-needle electrode electrical breakdown experiment findings

To study the difference between the high-voltage and low-voltage electrodes that did not penetrate the fracture pit during

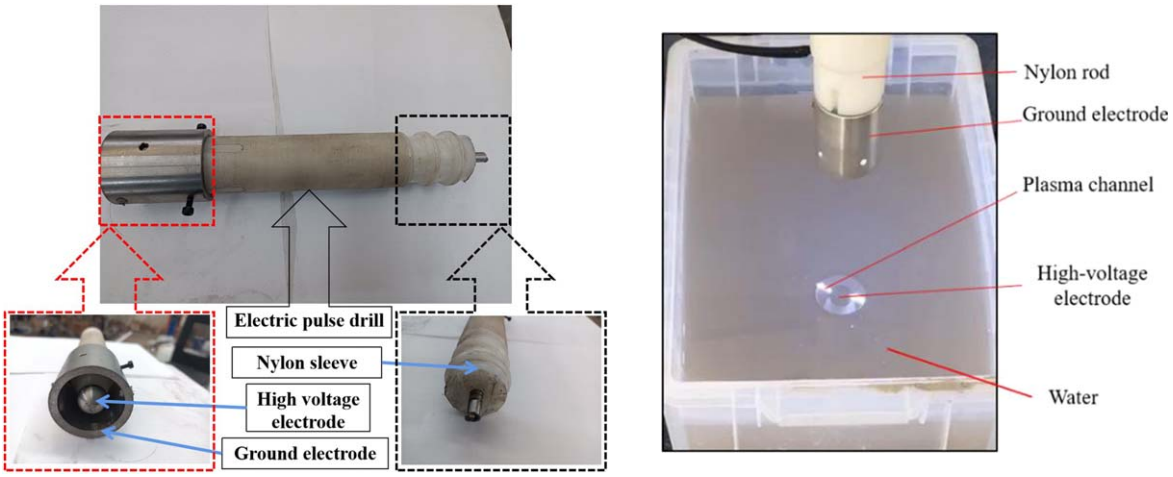

Figure 9. Structure diagram of HVEP drill.

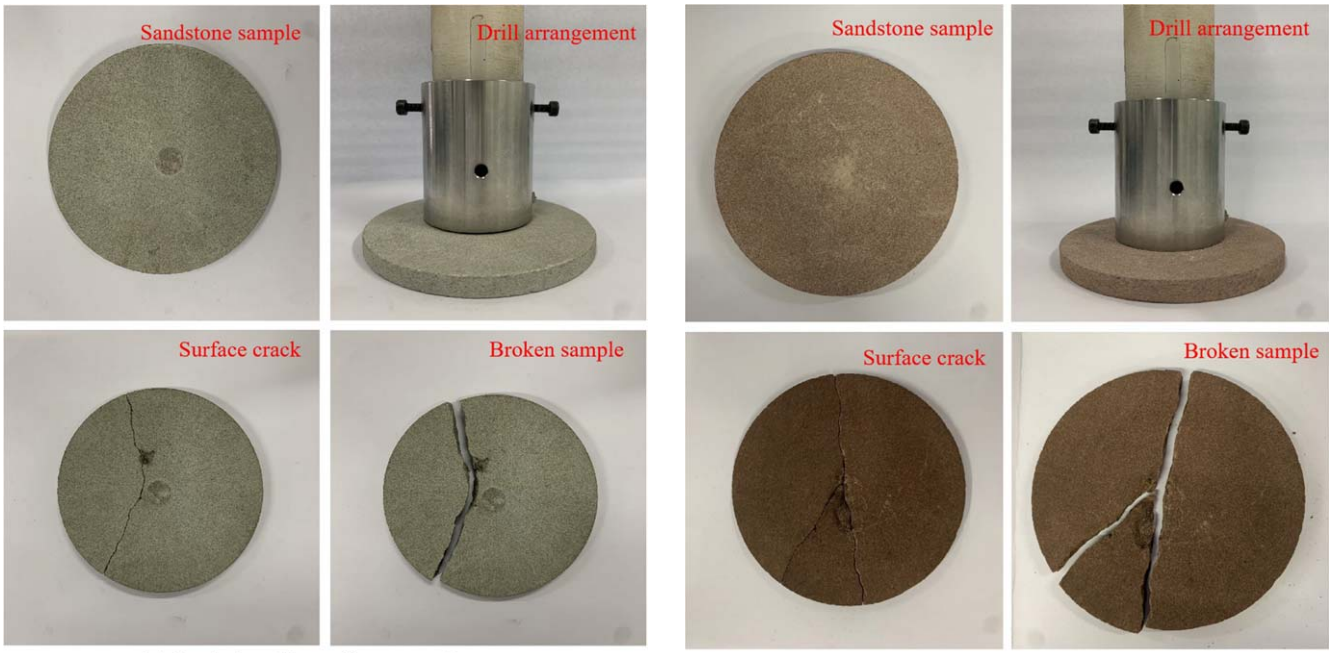

(a) Rock-breaking of gray sandstone **(b)** Rock-breaking of red sandstone

Figure 10. Process diagram of HVEP rock-breaking.

the HVEP rock-breaking process, the needle-needle electrodes were symmetrically arranged to conduct the electrical breakdown experiment, as shown in figure 12.

Because the fracture crater shape is presented near the high-voltage electrode and the grounding electrode, the findings indicate that the plasma channel sprouts from the end of the double electrodes (high-voltage electrode and grounding electrode) during the electric pulse discharge. This corresponds to the results of the electrical breakdown in the rock occurrence process depicted in figure 3 in section 4.1.

Rock samples devoid of penetrating fracture morphology were scanned with CT and x-ray to observe internal fracture features and the generation of plasma channels. During the experiment, a 3D reconstruction image x-ray microscope was utilized (MICROXCT-400). Figures 13 and 14 depict the CT pictures and 3D imaging results of fracture features of red and gray sandstone, respectively. Figures 13(a) and (b) represent, respectively, the positive pole and negative pole fracture craters of rock samples. Figure 13(c) reveals the CT scanning slices of rock samples, in which the portions with deeper gray levels represent pores, the portions with lighter gray levels represent argillaceous components in the rock, and the spots with lighter gray levels represent mineral particles within the rock. Figure 13(d) represents the CT scanning slices of rock samples, in which the portions with lighter gray levels represent mineral particles within the rock; the blue portion of the rock sample model displays the 3D imaging results of the internal fracture properties of the rock sample and the plasma channel shape.

Without piercing the broken shape, a plasma channel (or fissure) for charged particles to travel is generated in the rock. This is because, as discharge times rise, the limit of single

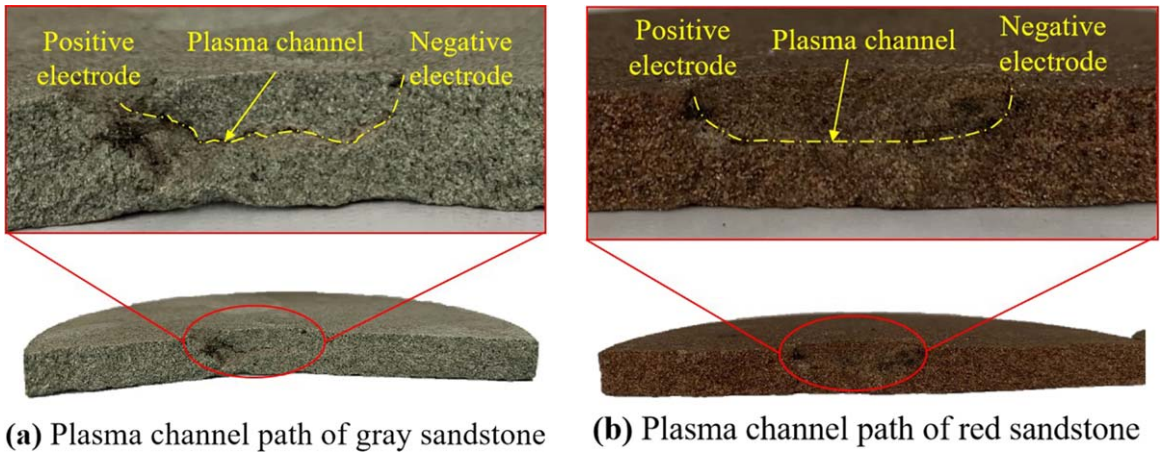

Figure 11. Schematic diagram of the HVEP plasma channel path in the experimental rock model.

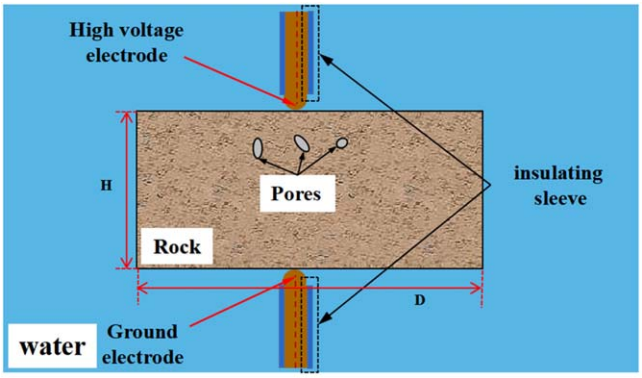

Figure 12. Schematic diagram of the electrical breakdown experiment with a needle-needle electrode symmetrically arranged.

pulse crushing is achieved at a certain point, and a plasma channel forms in the rock that completely penetrates the ends of the high-voltage and grounding electrodes. For the same kind of rock, the narrower the electrode spacing is, the easier it is to form plasma channels through the ends of high-voltage and grounding electrodes for the same end voltage load. When the broken shape is not penetrated, however, the broken degree of the crater on the positive electrode side is more significant than that on the grounding electrode side. This reveals that the development type of partial electrical breakdown is related to electrode polarity, which further proves the process of partial electrical breakdown.

Comparing figures 13 and 14, it is evident that the electrode end crushing degree (size of fracture crater) of gray sandstone is more extensive than that of red sandstone in rocks that do not penetrate the fracture crater. The rock's porosity may cause this phenomenon; the more significant the porosity, the greater the amount of conductive ions in the pores. Moreover, when the end voltage fluctuates often, the likelihood of partial discharge and electrolysis at the end of the rock increases proportionally.

To verify the hypothesis described above, the porosity of the two rocks was evaluated by immersing them in tap water. First, we determine the porosities of the two sandstones by comparing the quality of the samples before and after water immersion. The formula for calculating measured porosity is,

$$p = \frac{\Delta M}{M_1} \times \frac{\rho_R}{\rho_w} \times 100\% \tag{22}$$

where p is the measured porosity, %, ΔM is the quality of rock samples before and after immersion is poor, kg; ρ_w is the density of tap water; here we take ρ_w as 1000 kg m^{-3}; ρ_R is the rock density, the density of red sandstone is 2086.7 kg m^{-3}, while the density of gray sandstone is 2239.9 kg m^{-3}.

The measured porosities of red and gray sandstone are 8.49% and 12.07%, respectively. It is demonstrated that gray sandstone is more porous than red sandstone. Consequently, the larger the porosity of the gray sandstone, the greater the number of conductive ions present within its pores. Frequent modifications to the end voltage increase the probability of partial discharge and electrolysis at the rock's end. The degree of fragmentation (size of fracture crater) of the electrode end of the limestone is significantly greater than that of the electrode end of the red sandstone in the rock under the penetrating crushing shape, which is consistent with the conclusion reached in section 4.2. The greater the porosity, the greater the rock-breaking effect of electric pulse, and the easier it is to achieve the rock-breaking by the electric pulse.

6. Expectation

Specifically, the electrical breakdown numerical simulation model presented in this paper has the potential for development and improvement in the following areas: (1) the medium types in pores discussed in this paper are water and air/gas; oil should be considered when simulating the actual situation; (2) the influence of porosity and the proportion of pore fluid in the plasma channel is discussed, and other characteristics of pores inside a rock can be analyzed, such as pore shape, pore pressure, pore connectivity and pore multi-medium content; (3) the model can be used to study rock characteristic parameters (such as density, elastic modulus and Poisson's ratio), electrical parameters (internal impedance parameters of pulse transmitter, input power parameters, formation dielectric constant, drilling fluid and rock under the action of high-voltage pulses),

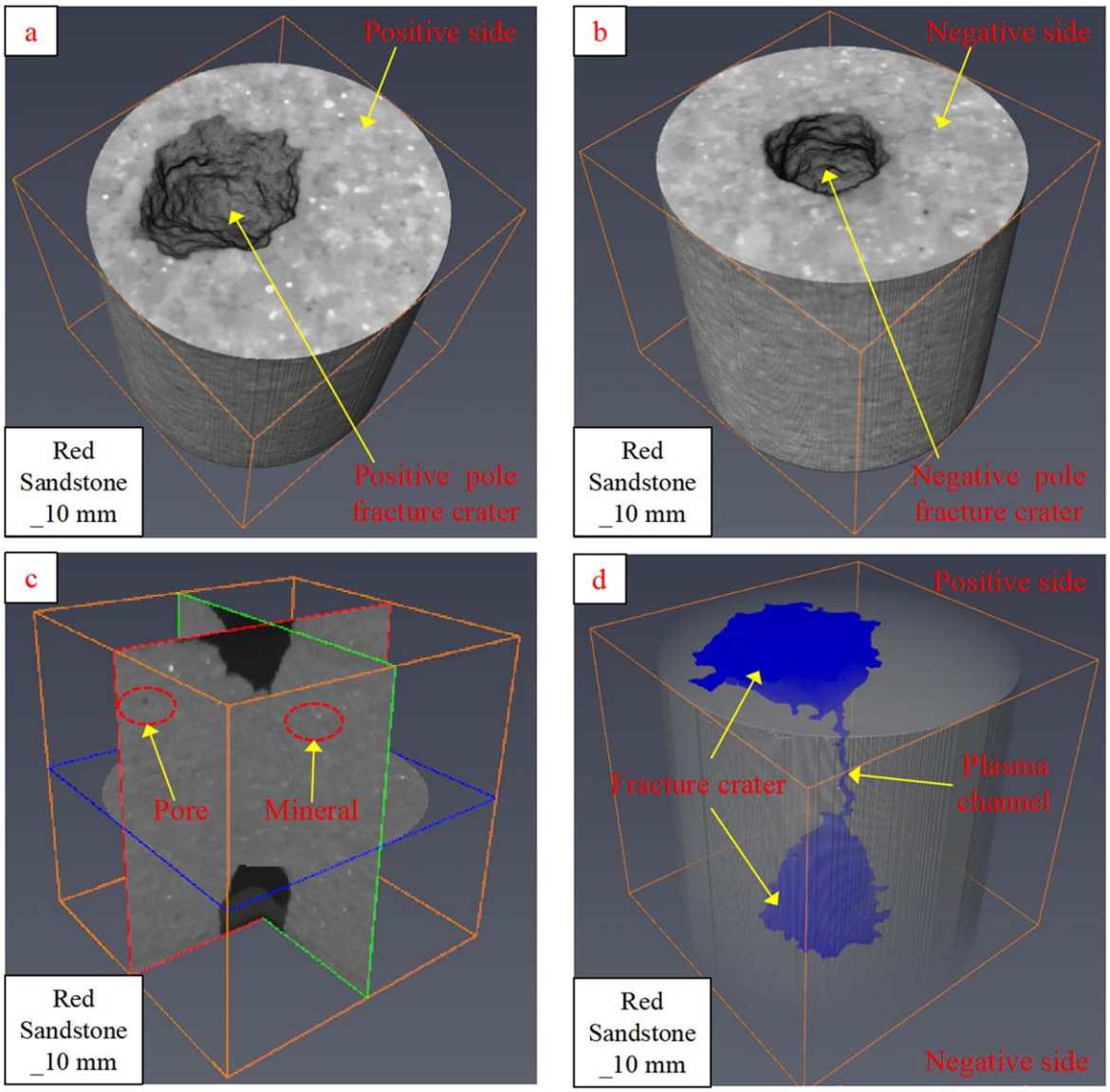

Figure 13. 3D imaging results of CT scanning and fracture characteristics of red sandstone.

conductivity, peak pulse voltage and pulse frequency, among others; (4) for this kind of rock crushing, the current is relatively high, so the magnetic field cannot be ignored under actual working conditions. The mechanical strength of rock should also be considered in this model, which is more appropriate to the actual situation. In forthcoming investigations, the factors mentioned above and the enhancement of the electrical breakdown model will be discussed.

7. Conclusion

To investigate the effect of pore characteristics on rock fragmentation by electric pulse, a numerical simulation model of electrical breakdown is developed by combining the four domains of circuit field, current field, breakdown field and solid mechanics. The possible conclusions are as follows:

(1) The electric field intensity will be distorted where there are pores in the rock, and the electrical breakdown channel will sprout from where the electric field strength is weak in the rock; the generation of a plasma channel has a specific 'directivity'. Electrical breakdown is more likely to occur as the internal porosity of the rock increases; as the internal porosity gradually increases, so does the electric field intensity in the 'electrical damage' area of the rock. The electric pulse's rock-breaking action will gradually strengthen as the porosity increases. The larger the porosity, the easier it is to perform the electric pulse rock-breaking.

(2) When the porosity of the rock model is fixed, the time required for the whole generation of the plasma channel under the action of an electric pulse falls gradually as the proportion of pore fluid drops; the corresponding failure area of the 'electrical damage' region inside the rock increases gradually as the proportion of pore fluid

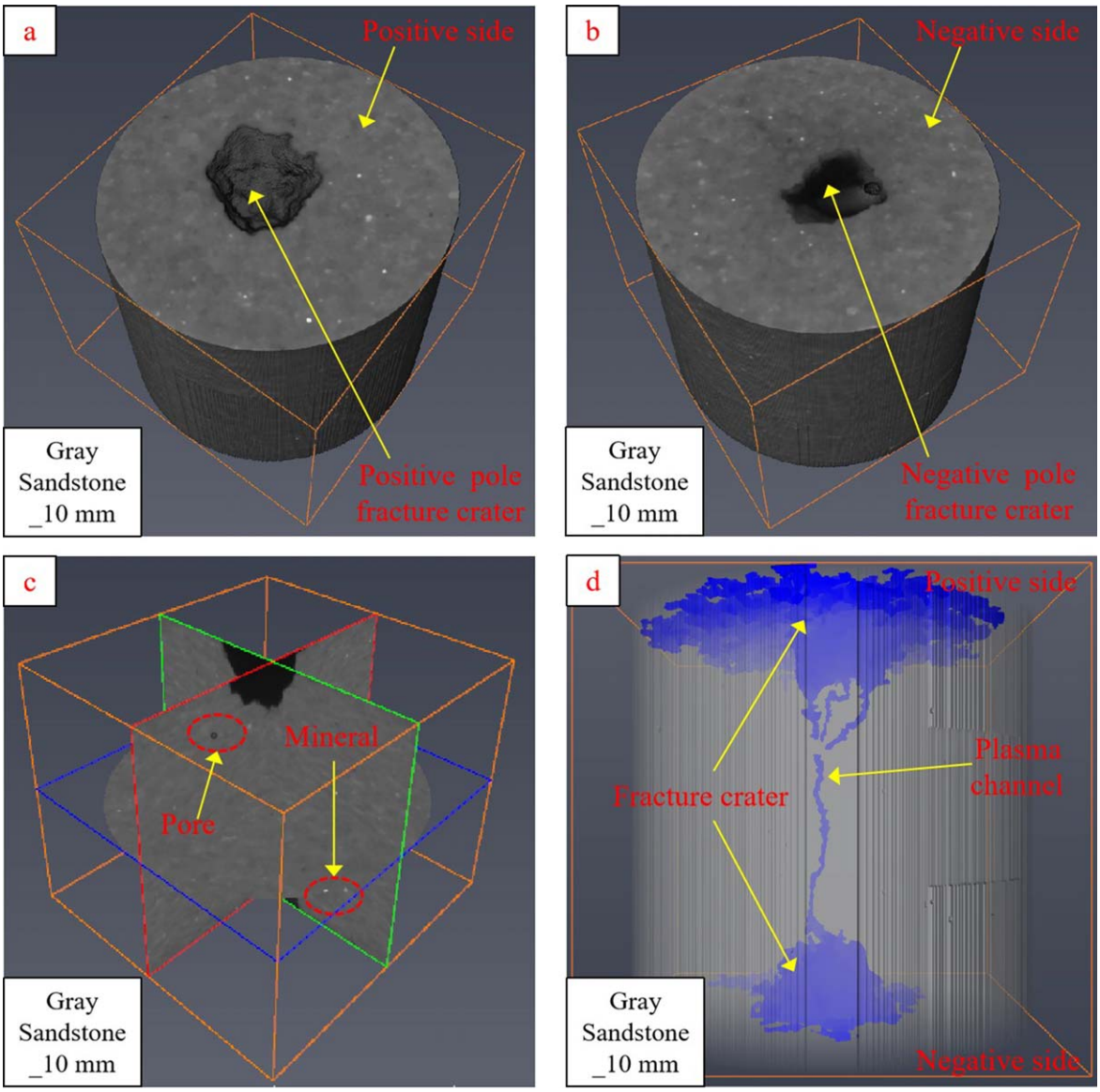

Figure 14. 3D imaging results of CT scanning and fracture characteristics of gray sandstone.

declines, which may more effectively promote the electric pulse rock-breaking for air. When the medium within the pores is merely air, the plasma channel route expands across the pores. However, when the medium in the pores is merely water, the plasma channel route extends along the surface of the pores.

(3) The plasma channel inside the rock is recreated by the laboratory experiment of HVEP, the rock along the course of the plasma channel has a distinct color difference from the surrounding rock because of the high energy (heat) in the channel, and the findings of the electrical breakdown experiment are consistent with the simulation test outcomes.

(4) The electrical breakdown tests with symmetrically positioned needle electrodes confirm that the plasma channel emerges from the ends of two electrodes (high-voltage electrode and grounding electrode) during the electric pulse discharge process. It is apparent that a high-voltage electrode has a larger fracture crater than a low-voltage electrode. The higher the porosity of the rock, the greater the possibility of partial discharge and electrolysis at its end, which further supports the theory that a partial electric shock is responsible for shattering rock.

Acknowledgments

This study is supported by National Natural Science Foundation of China (Nos. 52034006, 52004229, 52225401 and 52274231), Regional Innovation Cooperation Project of Sichuan Province (No. 2022YFQ0059), Natural Science Foundation of Sichuan Province (No. 23NSFSC2099) and Science and Technology Strategic Cooperation Project between Nanchong City and Southwest Petroleum University (No. SXHZ004).

References

[1] Gao D L 2003 *Explor. Eng.* **30** 8 (in Chinese)
[2] Tester J W *et al* 2007 *Philos. Trans. R. Soc. A Math. Phys. Eng. Sci.* **365** 1057
[3] Hu W R, Bao J W and Hu B 2013 *Pet. Explor. Dev.* **40** 439
[4] Diaz M B *et al* 2018 *Geothermics* **72** 348
[5] Meng F Z, Wong L N Y and Guo T Y 2022 *Tectonophysics* **842** 229589
[6] Schiegg H O *et al* 2015 *J. Earth Sci.* **26** 37
[7] Kusaiynov K *et al* 2017 *Tech. Phys.* **62** 867
[8] Vogler D *et al* 2020 *Acta Geotech.* **15** 2327
[9] Rossi E *et al* 2020 Advanced drilling technologies to improve the economics of deep geo-resource utilization *2nd Applied Energy Symp.: MIT A+B (MITAB 2020) (Boston)* (ETH Zurich, Geothermal Energy & Geofluids) p 148
[10] Timoshkin I V, Mackersie J W and MacGregor S J 2004 *IEEE Trans. Plasma Sci.* **32** 2055
[11] Biela J *et al* 2009 *IEEE Trans. Dielectr. Electr. Insul.* **16** 1093
[12] Zhu X H, Luo Y X and Liu W J 2020 *J. Petrol. Sci. Eng.* **194** 107356
[13] Anders E, Lehmann F and Voigt M 2015 Electric impulse technology: long run drilling in hard rocks *ASME 2015 34th Int. Conf. on Ocean, Offshore and Arctic Engineering (St. John's)* (American Society of Mechanical Engineers) V010T11A008
[14] Anders E *et al* 2017 Electric impulse drilling: the future of drilling technology begins now *ASME 2017 36th Int. Conf. on Ocean, Offshore and Arctic Engineering (Trondheim)* (American Society of Mechanical Engineers) V008T11A024
[15] Ito M *et al* 2009 *Int. J. Miner. Process.* **92** 7
[16] Vazhov V F *et al* 2010 *Tech. Phys.* **55** 833
[17] Vazhov V F *et al* 2014 *J. Phys.: Conf. Ser.* **552** 012050
[18] Razavian S M, Rezai B and Irannajad M 2014 *Adv. Powder Technol.* **25** 1672
[19] Zuo W R, Shi F N and Manlapig E 2014 *Miner. Eng.* **69** 196
[20] Andres U 1995 *Miner. Process. Extr. Metall. Rev.* **14** 87
[21] Andres U 2010 *Int. J. Miner. Process.* **97** 31
[22] Mesyats G A 2005 *Tech. Phys. Lett.* **31** 1061
[23] Ho C C *et al* 2014 *Meas. Sci. Technol.* **25** 094007
[24] Fujita T *et al* 2001 *Eur. J. Miner. Process. Environ. Prot.* **1** 113
[25] Li C P *et al* 2019 *Energies* **12** 727
[26] Li C P *et al* 2020 *J. Nat. Gas Sci. Eng.* **77** 103263
[27] Li C P *et al* 2021 *J. Nat. Gas Sci. Eng.* **86** 103730
[28] Jorden J R and Campbell F L 1985 *Well Logging: Rock Properties, Borehole Environment, Mud and Temperature Logging* (Dallas, TX: Society of Petroleum Engineers)
[29] Lin Y X *et al* 2022 *J. Nat. Gas Sci. Eng.* **104** 104684
[30] Amyx J W, Bass D M and Whiting R L 1960 *Petroleum Reservoir Engineering: Physical Properties* (New York: McGraw-Hill)
[31] Barton N 2006 *Rock Quality, Seismic Velocity, Attenuation and Anisotropy* (London: CRC Press)
[32] Ezzat M *et al* 2022 *Energies* **15** 250
[33] Bai L L *et al* 2021 *SPE Oil Gas Reservoirs* **28** 148 (in Chinese)
[34] Jonscher A K and Lacoste R 1984 *IEEE Trans. Electr. Insul.* **EI-19** 567
[35] Lisitsyn I V *et al* 1998 *J. Appl. Phys.* **84** 6262
[36] Zhu X H *et al* 2020 *Acta Petrol. Sin.* **41** 1146 (in Chinese)
[37] Zhu X H *et al* 2021 *Rock Mech. Rock Eng.* **54** 4593
[38] Boev S *et al* 1999 Destruction of granite and concrete in water with pulse electric discharges *Digest of Technical Papers. 12th IEEE Int. Pulsed Power Conf. (Cat. No.99CH36358) (Monterey)* (IEEE) p 1369
[39] Boev S *et al* 1997 Electropulse technology of material destruction and boring *Digest of Technical Papers. 11th IEEE Int. Pulsed Power Conf. (Cat. No.97CH36127) (Baltimore)* (IEEE) p 220
[40] Lisitsyn I V *et al* 1999 Drilling and demolition of rocks by pulsed power *Digest of Technical Papers. 12th IEEE Int. Pulsed Power Conf. (Cat. No.99CH36358) (Monterey)* (IEEE) p 169
[41] Inoue H *et al* 1999 *Jpn. J. Appl. Phys.* **38** 6502
[42] Song K Y *et al* 2009 *J. Micromech. Microeng.* **19** 045006
[43] Zhang Z C *et al* 2012 *High Voltage Eng.* **38** 1719 (in Chinese)
[44] Zhang Z C 2013 Rock fragmentation by pulsed high voltage discharge and drilling equipment development *PhD Thesis* Zhejiang University, Hangzhou, China (in Chinese)
[45] Molchanov D V and Lavrinovich I V 2019 *J. Phys. Conf. Ser.* **1172** 012069
[46] Petrov Y V *et al* 2015 *Tech. Phys.* **60** 1733
[47] Ezzat M *et al* 2021 *Energies* **14** 4717
[48] Husain E and Nema R S 1982 *IEEE Trans. Electr. Insul.* **EI-17** 350
[49] Slade P G and Taylor E D 2002 *IEEE Trans. Compon. Packag. Technol.* **25** 390
[50] Tirumala R and Go D B 2010 *Appl. Phys. Lett.* **97** 151502
[51] Loveless A M *et al* 2019 *Sci. Rep.* **9** 5669